NGC300 X-1 is a Wolf-Rayet/Black-Hole binary

Journal Item

Monthly Notices of the Royal Astronomical Society LETTERS

Mon. Not. R. Astron. Soc. **403,** L41–L45 (2010) doi:10.1111/j.1745-3933.2010.00811.x

NGC 300 X-1 is a Wolf–Rayet/black hole binary★

P. A. Crowther,[1]† R. Barnard,[2] S. Carpano,[3] J. S. Clark,[2] V. S. Dhillon[1] and A. M. T. Pollock[3]

[1]*Department of Physics and Astronomy, University of Sheffield, Sheffield S3 7RH*
[2]*Department of Physics and Astronomy, The Open University, Walton Hall, Milton Keynes MK7 6AA*
[3]*XMM–Newton Science Operations Center, ESAC, 28080, Madrid, Spain*

Accepted 2010 January 6. Received 2010 January 6; in original form 2009 November 20

ABSTRACT

We present Very Large Telescope/FORS2 time-series spectroscopy of the Wolf–Rayet (WR) star #41 in the Sculptor group galaxy NGC 300. We confirm a physical association with NGC 300 X-1, since radial velocity variations of the He II λ4686 line indicate an orbital period of 32.3 ± 0.2 h which agrees at the 2σ level with the X-ray period from Carpano et al. We measure a radial velocity semi-amplitude of 267 ± 8 km s^{-1}, from which a mass function of 2.6 ± 0.3 M$_\odot$ is obtained. A revised spectroscopic mass for the WN-type companion of 26^{+7}_{-5} M$_\odot$ yields a black hole mass of 20 ± 4 M$_\odot$ for a preferred inclination of 60°–75°. If the WR star provides half of the measured visual continuum flux, a reduced WR (black hole) mass of $15^{+4}_{-2.5}$ M$_\odot$ ($14.5^{+3}_{-2.5}$ M$_\odot$) would be inferred. As such, #41/NGC 300 X-1 represents only the second extragalactic WR plus black hole binary system, after IC 10 X-1. In addition, the compact object responsible for NGC 300 X-1 is the second highest stellar-mass black hole known to date, exceeded only by IC 10 X-1.

Key words: stars: Wolf–Rayet – galaxies: individual: NGC 300 – X-rays: binaries – X-rays: individual: NGC 300 X-1.

1 INTRODUCTION

High mass X-ray binaries (HMXB) typically comprise OB stars plus either a neutron star or a black hole, in which high X-ray luminosities (∼10^{38} erg s^{-1}) arise from accretion discs around the compact object. Accretion discs are fed through a combination of Roche-lobe overflow and stellar winds from the early-type companion. Very few known HMXB are known to host black holes, Cyg X-1 in the Milky Way, X-1 and X-3 in the Large Magellanic Cloud (LMC) and X-7 in the Local Group galaxy M33. If a merger is avoided, the OB companion will potentially evolve through to a Wolf–Rayet (WR) phase, producing a system comprising a helium star plus a black hole or neutron star (Tutukov & Yungelson 1973). Indeed, van den Heuvel & de Loore (1973) proposed the Galactic HMXB Cyg X-3 as a helium star plus compact object system, which was observationally confirmed by van Kerkwijk et al. (1992). Such systems are believed to be very rare, with as few as ∼100 helium star plus black hole pairs in the Galaxy (Ergma & Yungelson 1998).

To date, the only confirmed WR plus black hole binary system is IC 10 X-1 in the dwarf irregular galaxy IC 10. This system has a period of 34.9 h, hosts a WN-type WR star [MAC 92] 17A (Crowther et al. 2003) and an unseen companion which is currently the record holder amongst stellar-mass black holes, exceeding 23.1 ± 2.1 M$_\odot$ (Prestwich et al. 2007; Silverman & Filippenko 2008).

A second candidate extragalactic black hole plus WR system is NGC 300 X-1 (Carpano et al. 2007a), in the southern Sculptor group spiral galaxy NGC 300 which lies at a distance of 1.88 Mpc (Gieren et al. 2005). This source is spatially coincident with #41 from the WR catalogue of Schild et al. (2003) which was confirmed as a WN-type WR star by Crowther et al. (2007). Both systems exhibit similar X-ray properties (Carpano et al. 2007b; Barnard, Clark & Kolb 2008). However, no evidence exists to date of a physical link between NGC 300 X-1 and the WR star #41. This is the purpose of this Letter.

New Very Large Telescope (VLT) optical spectroscopic time-series of #41 are discussed in Section 2 in which variations are revealed in the He II λ4686 emission line. Section 3 compares the inferred orbital period with X-ray light curves and derives a semi-amplitude for the WR star, from which a mass function is obtained. Section 4 provides a revised mass for the WR star, placing strict limits upon the mass of the compact companion. We conclude with a brief discussion in Section 5.

2 OBSERVATIONS

Here we present new VLT optical spectroscopy of #41 obtained with the Focal Reducer/Low Dispersion Spectrograph #2 (FORS2)

★Based on observations made with European Southern Observatory (ESO) telescopes at the Paranal Observatory under programme ID 384.D-0093(A).
†E-mail: Paul.crowther@sheffield.ac.uk

Table 1. Log of VLT/FORS2 spectroscopic observations of #41 in NGC 300. UT dates and MJDs refer to the start of the 1535 s exposures. We include individual radial velocities, v_r, as measured from Gaussian fits to He II λ4686. Phases adopt a period of 32.3 h, where phase 0 refers to MJD 55118.975 59 ± 0.015 54.

UT Date	MJD −55119	DIMM (arcsec)	sec z	v_r λ4686 (km s^{-1})	Phase
01:06 2009 Oct 15	0.046 180	1.2	1.29	347.0 ± 17.7	0.052
05:28 2009 Oct 15	0.227 922	2.3	1.08	364.6 ± 25.5	0.187
01:40 2009 Oct 16	1.069 495	1.1	1.18	−64.2 ± 16.9	0.812
05:58 2009 Oct 16	1.249 073	1.7	1.14	136.0 ± 25.0	0.945
04:07 2009 Oct 19	4.171 590	0.7	1.03	369.0 ± 14.3	0.114
08:24 2009 Oct 19	4.350 382	0.8	1.98	456.6 ± 20.1	0.247
02:31 2009 Oct 20	5.104 896	0.9	1.06	−68.3 ± 12.1	0.807
06:41 2009 Oct 20	5.278 856	0.7	1.31	109.4 ± 17.3	0.936
00:14 2009 Oct 25	10.010 318	1.2	1.34	325.3 ± 25.7	0.447
06:28 2009 Oct 25	10.269 520	0.7	1.33	10.4 ± 14.3	0.639

in a multi-object spectroscopy (MOS) mode from 2009 October 14–24. Two 1535 s exposures were obtained on each of five non-consecutive nights using the 600B grism, centred at 465 nm. A log of our observations is presented in Table 1 including differential image motion monitor (DIMM) seeing measurements, which indicated a typical seeing of 0.7–1.2 arcsec, except at two epochs for which the seeing exceeded 1.5 arcsec.

MOS allows 19 sources to be simultaneously observed. We included seven H II regions in NGC 300 plus 12 WR candidates from Schild et al. (2003). Of these, three sources have previously been spectroscopically confirmed as WR stars, namely #9, #41 and source 12 from Bresolin et al. (2009). Other sources will be discussed elsewhere.

After bias subtraction and flat-field correction, a standard extraction was performed using IRAF, with wavelength and flux calibration carried out using FIGARO. 1.0 arcsec slits provided a spectral resolution of 4.2 Å – as measured from comparison arc lines – with a wavelength coverage of 3300–5800 Å for #41. Faint Hβ and [O III] λλ4959, 5007 nebular lines were detected in the #41 slit. #41 does not appear to be responsible for these features since the intensity of the nebula is weak and spatially close to #41, and has a lower systemic velocity of ∼95 km s^{-1} (versus 202 km s^{-1} for #41).

Spectrophotometric standard stars were observed with FORS2 in a long slit mode on the nights of October 15 (HD 49798), October 18–19 (LTT 2415) and October 24 (LTT 7987), providing a wavelength coverage of 3300–6230 Å. An absolute flux calibration was achieved for #41 using $B = 22.71$ mag from Carpano (2006).

3 ORBITAL PERIOD

Several VLT/FORS2 spectroscopic observations in the vicinity of He II λ4686 are presented in Fig. 1, revealing large radial velocity variations. Gaussian profiles are fitted to individual λ4686 profiles, with individual centroids listed in Table 1.

In view of the sparsely sampled data sets, we have employed the string-length approach of Dworetsky (1983). The data are folded on a set of trial frequencies and the total length of 'string' required to join the observations in phase order is calculated. The smallest string length found from the search is assumed to correspond to the correct period. The resulting periodogram is shown in Fig. 2. The deepest trough corresponds to a period of 32.3 ± 0.2 h. The error on this period was computed by constructing 10 000 synthesized data sets and measuring the standard deviation of the positions of the deepest

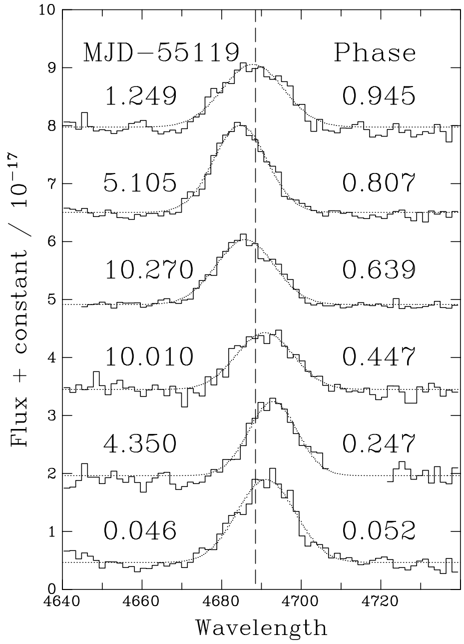

Figure 1. Representative VLT/FORS2 spectroscopy of #41 revealing radial velocity variations in He II λ4686 (Gaussian fits are shown as dotted lines), successively offset by 1.5×10^{-17} erg s^{-1} cm^{-2} Å^{-1} for clarity.

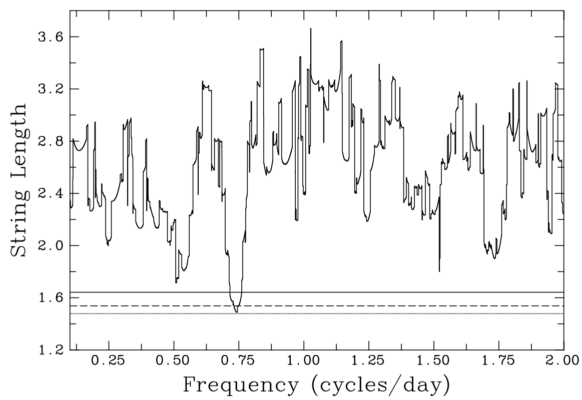

Figure 2. String-length periodogram of the VLT/FORS2 radial velocities. The minimum string length indicates the best period, at a frequency of 0.7422 cycles/day. The solid, dashed and dotted lines represent the 68.3, 95.4 and 99.7 per cent confidence levels, respectively (see text for details).

troughs in the resulting periodograms. The synthesized data sets were obtained by 'jiggling' each data point about its observed value by an amount given by its error bar multiplied by a number output by a Gaussian random-number generator with zero mean and unit variance.

It can be seen that our derived period is in agreement at the 2σ level with the *Swift* X-ray period of 32.8 ± 0.2 h (1σ; Carpano et al. 2007b), which gives us confidence that we have identified the correct value. Moreover, the minimum string length of our period (1.49) compares favourably with the string length of a perfect sinusoid (1.46) and the string length of a sinusoid with noise consistent with the error bars on the observed data added to it (1.48).

To further test the significance of our derived period, we used a randomization technique (Fisher 1935). The radial velocities were randomly reassigned to the times of observation, thereby preserving the data sampling and the mean and standard deviation of the

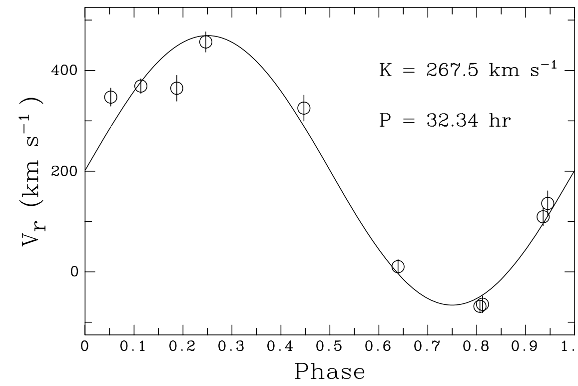

Figure 3. Radial velocity variations of λ4686 He II phased to 32.3 h, from which a systemic velocity of $v_r = 202 \pm 7\,\mathrm{km\,s^{-1}}$ and semi-amplitude of $K_2 = 267.5 \pm 7.7\,\mathrm{km\,s^{-1}}$ are obtained.

original data set. A set of 10 000 randomized data sets were constructed in this way and then subjected to the same string-length periodogram analysis. By constructing a cumulative distribution function of the resulting minimum string lengths, we are able to place confidence limits on the significance of a given string length, as shown by the horizontal lines in Fig. 2. We are able to reject the hypothesis that our preferred period is due to noise at 99.43 per cent confidence and eliminate the next highest troughs as most likely due to noise. Note that the troughs around 0.25 and 1.75 cycles/day are due to the one-cycle-per-day alias. As a check on the string-length method, we also computed a Lomb–Scargle periodogram (Press & Rybicki 1989) and obtained consistent results.

Adopting our optical period, we present the phased radial velocity measurements in Fig. 3, with a semi-amplitude of $K_2 = 267.5 \pm 7.7\,\mathrm{km\,s^{-1}}$. In the figure, phase 0 corresponds to MJD 55118.975 59±0.015 54.

Armed with the semi-amplitude and orbital period, we may now derive the system mass function,

$$f(m) = \frac{P K_2^3}{2\pi G} = \frac{M_1 \sin^3 i}{(1+q)^2},$$

where M_1 is the compact object mass and $q = M_2/M_1$. The derived mass function is $f(m) = 2.63 \pm 0.33\,\mathrm{M_\odot}$ and would correspond to the compact object mass in the case of a system viewed at an inclination of 90° whose companion mass is negligible. In the case of a massive companion star with $q \sim 1$, the compact object would have a minimum mass of $4f(m)$. As such, the compact object in NGC 300 X-1 is indeed a black hole, such that this system represents only the second confirmed WR plus black hole binary.

4 WOLF–RAYET PROPERTIES

We present our new, combined (phase-corrected), rectified VLT/FORS2 spectrum of #41 in Fig. 4. This high quality spectrum confirms a weak-lined WN5 subtype, previously inferred by Crowther et al. (2007) from lower resolution, lower signal-to-noise ratio (S/N) spectroscopy obtained with VLT/FORS2 using the 300V grism in 2007 January. Overall, the visual spectrum of #41 is similar to other weak-lined WN5 stars, namely WR 49 in the Milky Way and Brey 65b (=NGC 2044 West 5C) in the LMC, taken from Hamann, Koesterke & Wessolowski (1995) and Walborn et al. (1999), respectively. The He II λ4686 equivalent width ($W_\lambda \sim 56$ Å) and linewidth [full width at half-maximum (FWHM) ∼ 17 Å] in #41

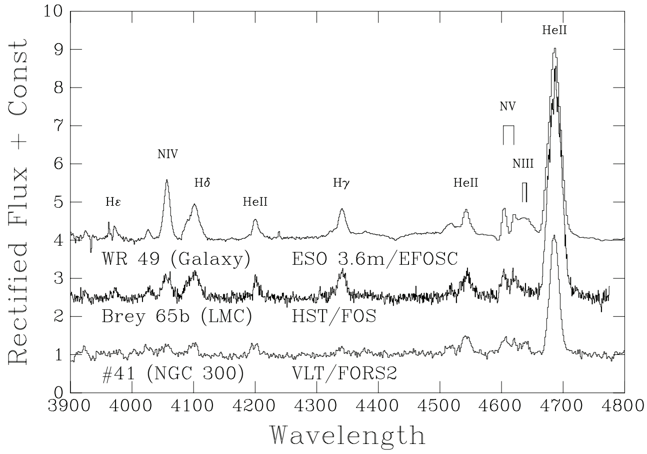

Figure 4. Comparison between rectified, phase-corrected VLT/FORS2 spectrum of #41 with Galactic (WR 49) and LMC (Brey 65b = NGC 2044 West 5C) weak-lined WN5 stars, respectively, from Hamann et al. (1995) and Walborn et al. (1999).

are somewhat lower than LMC and Milky Way counterparts, W_λ = 110–140 Å and FWHM = 22–24 Å.

In order to reassess the mass of #41, we have calculated a synthetic model using the Hillier & Miller (1998) line-blanketed, non-local thermodynamic equilibrium model atmosphere code. With respect to Crowther et al. (2007), somewhat more sophisticated atomic models are considered, namely H, He, C, N, O, Ne, Si, P, S, Ar, Fe and Ni. Elemental abundances are set to 40 per cent of the solar value (Urbaneja et al. 2005), with the exception of H and CNO elements. Clumping is accounted for, albeit in an approximate manner, with a (maximum) volume filling factor of 10 per cent, such that the derived mass-loss rate is three times smaller than the value that would have been obtained by assuming a homogeneous wind.

In view of the weak He I line spectrum in #41, we have based our analysis upon He II (λλ4686, 5411) and N IV–V (λλ4603–4620, λ4058, λλ7103–7129) line diagnostics. Overall good agreement is found, which is remarkable in view of the close proximity of the black hole to #41. The only significant discrepancies are that N III λλ4634–4641 is not reproduced in the synthetic spectrum and excess emission is observed in the upper Pickering–Balmer series, the latter potentially arising from the accretion disc.

In Fig. 5 we present our new combined flux-calibrated spectrum of #41, together with recalibrated spectroscopy from Crowther et al. (2007) for λ > 5800 Å. An optimum fit to the spectrum of #41 is included in the figure and reveals the following stellar parameters: $T_* \sim 65$ kK, $\log(L/L_\odot) \sim 5.92$, $\dot{M} \approx 5 \times 10^{-6}\,\mathrm{M_\odot\,yr^{-1}}$, $v_\infty \sim 1300\,\mathrm{km\,s^{-1}}$, plus a nitrogen mass fraction of ∼0.5 per cent, with negligible hydrogen adopted. With respect to Crowther et al. (2007), the main revision relates to a reduced absolute magnitude of $M_V = -5.0$ mag, on the basis of a lower interstellar reddening of $E(B-V) = 0.4$ mag. T_* should be reliable to ±5 kK, resulting in uncertainties of ±0.2 mag in bolometric corrections. Together with ±0.05 mag uncertainties in $E(B-V)$, stellar luminosities should be reliable to ±0.14 dex.

From our derived parameters, we obtain a spectroscopic WR mass of $26^{+7}_{-5}\,\mathrm{M_\odot}$ on the basis of the Schaerer & Maeder (1992) mass–luminosity relation for hydrogen-free WR stars. The principal uncertainty in our inferred WR mass relates to the absolute visual magnitude of the WR star. Since our adopted visual magnitude is based upon ground-based imaging, it is possible that other continuum sources are included in the photometry. In this case, the WR

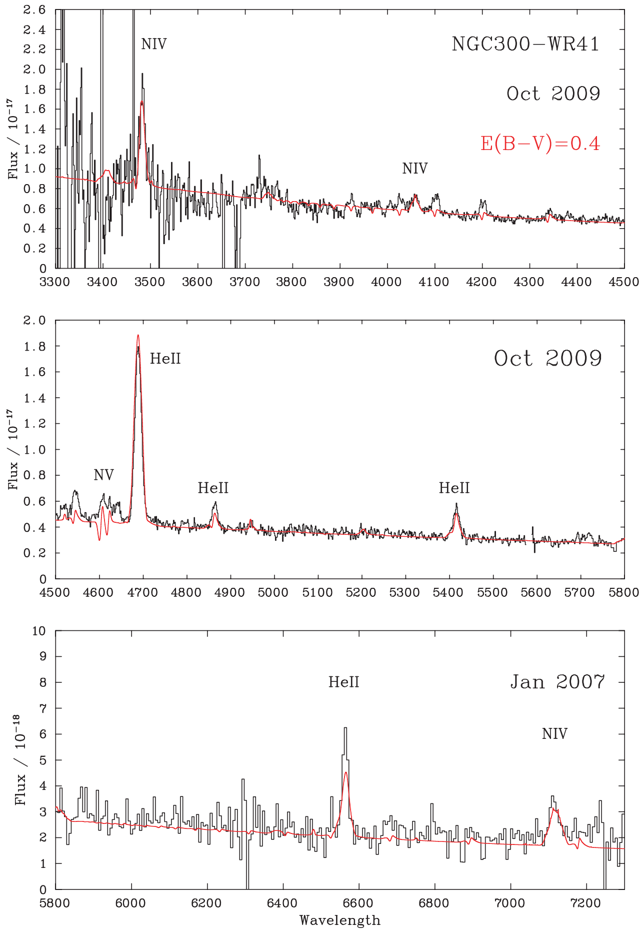

Figure 5. Combined, phase-corrected VLT/FORS2 spectroscopy of #41 from 2009 October and 2007 January (black) with the synthetic spectrum overlaid (red), reddened by $E(B-V) = 0.4$ mag, as described in Section 4.

emission-line-equivalent width would be diluted by the continuum of other nearby sources.

Indeed, while #41 closely resembles other weak-lined WN5 stars (recall Fig. 4), its He II λ4686 equivalent width is indeed lower by a factor of ∼2. This hints at a potential factor of 2 line dilution from unresolved companions along the sightline towards #41. In this case, the WR luminosity would be reduced to $\log{(L/L_\odot)} = 5.57 \pm 0.14$ with the mass-loss rate unaffected, implying a spectroscopic mass of $15^{+4}_{-2.5}$ $M_\odot$. For reference, Hamann, Gräfener & Liermann (2006) estimated spectroscopic masses of 15–19 $M_\odot$ for weak-lined WN5 stars in the Milky Way. In view of these issues, we shall evaluate black hole masses using values of both 15 and 26 $M_\odot$ for the WN star.

5 DISCUSSION AND CONCLUSIONS

In Table 2 we present black hole masses for inclinations of 45°, 60° and 90° for our favoured 26 $M_\odot$ spectroscopic WR mass, plus the 15 $M_\odot$ case, resulting from the WR star contributing 50 per cent of the visual continuum light. We include the separation between the components using Kepler's third law in each case, obtained from

$$P = \frac{2\pi a^{3/2}}{[G(M_1 + M_2)]^{1/2}},$$

corresponding to only 2.5–3.5 WR radii.

Table 2. Derived black hole mass, M_1, in NGC 300 X-1 for $i = 45°$, 60° or 90°, for cases in which the WN star contributes either 50 per cent ($M_2 = 15\,M_\odot$) or 100 per cent ($M_2 = 26\,M_\odot$) of the visual light. We include the separation between the components, a, and the WR radius, R_2, as a fraction of the Roche-lobe radius, r_L (Eggleton 1983).

M_2 (WR) ($M_\odot$)	R_2 (WR) ($R_\odot$)	i	M_1 (BH) ($M_\odot$)	a ($R_\odot$)	R_2/r_L
$15^{+4}_{-2.5}$	4.8±0.1	45[a]	$21.5^{+2.5}_{-1.7}$	$17.0^{+0.9}_{-0.7}$	0.81
$15^{+4}_{-2.5}$	4.8±0.1	60	$15.6^{+1.9}_{-1.4}$	$16.1^{+1.0}_{-0.7}$	0.80
$15^{+4}_{-2.5}$	4.8±0.1	90[a]	$12.6^{+1.6}_{-1.3}$	$15.5^{+1.0}_{-0.8}$	0.79
26^{+7}_{-5}	7.2±0.1	45[a]	$27.8^{+3.5}_{-2.8}$	$19.4^{+1.2}_{-1.0}$	0.99
26^{+7}_{-5}	7.2±0.1	60	$20.6^{+2.9}_{-2.1}$	$18.5^{+1.3}_{-1.0}$	0.98
26^{+7}_{-5}	7.2±0.1	90[a]	$16.9^{+2.4}_{-1.9}$	$18.0^{+1.2}_{-1.0}$	0.96

[a]The apparent glancing eclipse of the X-ray emitting accretion disc suggests $i = 60°–75°$.

The mass accretion rate required to sustain $L_X = 2 \times 10^{38}$ erg s^{-1} is $3.5 \times 10^{-8}\,M_\odot$ yr^{-1}, if the adopted efficiency of gravitational release is ∼10 per cent (see Shakura & Sunyaev 1973). This is ≤1 per cent of our derived mass-loss rate of #41. However, Table 2 also shows that the WR star would completely fill its Roche lobe for the 26 $M_\odot$ case ($i \leq 35°$ is excluded) and equates to 80 per cent of its Roche-lobe radius, r_L (Eggleton 1983), for the 15 $M_\odot$ case. Therefore, the accretion disc may be fed primarily through Roche-lobe overflow. For comparison, the higher temperature obtained for the WN star in IC 10 X-1 by Clark & Crowther (2004) would favour a wind-fed accretion disc, since the WR radius is $\sim 0.5 r_L$ in that system.

IC 10 X-1 is an eclipsing X-ray system (Prestwich et al. 2007); therefore, geometric arguments imply that the black hole would be eclipsed for $i \geq 78°$ for the WR properties derived by Clark & Crowther (2004). If we adopt a radius of $\sim 0.5\, r_L$ for the accretion disc, an eclipse of the X-ray emitting accretion disc would require $i \geq 80°$. NGC 300 X-1 does exhibit significant X-ray variability, but lacks a deep X-ray eclipse (Carpano et al. 2007b). Therefore, geometric arguments appear to rule out inclinations that would cause a total eclipse of the accretion disc ($i \leq 73° \pm 2°$). However, a glancing eclipse would require $i \geq 63.\!\!^\circ5 \pm 3.\!\!^\circ5$ for the range of WR radii obtained here. We therefore adopt $i = 80°–90°$ for IC 10 X-1 and $i = 60°–75°$ for NGC 300 X-1.

In Fig. 6 we present the host galaxy metallicity as a function of black hole masses for NGC 300 X-1 and IC 10 X-1, plus those for all HMXB systems for which the presence of a black hole is unambiguous, whose companion is an OB star with mass $M_2 \geq 5\,M_\odot$, i.e. LMC X-3 (Val-Baker, Norton & Negueruela 2007), LMC X-1 (Orosz, Steeghs & McClintock 2009), M33 X–7 (Orosz et al. 2007), V4641 Sgr (Orosz et al. 2001) and Cyg X-1 (Gies et al. 2003). We limit our sample to classical HMXB, to ensure that their present-day (oxygen) metallicities are consistent with the formation of these black hole binaries. The majority of black holes in low mass X-ray binary systems have masses close to 10 $M_\odot$ (Remillard & McClintock 2006).

It may be significant that both WR/black hole systems are located in metal-poor galaxies. IC 10 has an oxygen content of log (O/H) + 12 = 8.1 (Garnett 1990) while NGC 300 X-1/#41 is located at a deprojected distance of 0.43 ρ_0, where $\rho_0 = 9.75$ arcmin (Schild et al. 2003). According to Urbaneja et al. (2005), the oxygen content at this galactocentric distance in NGC 300 is log (O/H) + 12 ∼ 8.44,

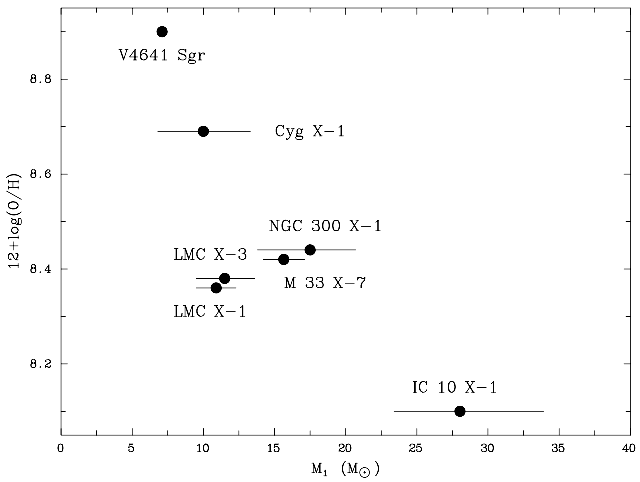

Figure 6. Comparison between inferred compact object masses, M_1, versus metallicity for all HMXB with $M_1 \geq 3\,M_\odot$ and $M_2 \geq 5\,M_\odot$. Black hole masses inferred for NGC 300 X-1 (IC 10 X-1) relate to a WR mass of $21^{+5}_{-6}\,M_\odot$ ($25^{+13}_{-8}\,M_\odot$) and an orbital inclination of 60°–75° (80°–90°).

i.e. relatively similar to the LMC for which log(O/H) + 12 ∼ 8.37 (Russell & Dopita 1990). The only other HMXB whose black hole mass is known to greatly exceed $10\,M_\odot$ is M33 X-7 (Orosz et al. 2007), for which a near identical oxygen content of log (O/H) + 12 = 8.42 is inferred at its location in M33 from the calibration of Magrini et al. (2007).

High black hole masses require that the progenitor star was very massive and experienced low mass-loss rates (Belczynski et al. 2009). Weak stellar winds is a natural consequence of low metallicity (Mokiem et al. 2007). However, orbital periods of IC 10 X-1 and NGC 300 X-1 are so short that the radius of the black hole progenitor star must have been larger than the present separation of the components. As such, the progenitor would have experienced extreme mass loss through Roche-lobe overflow. Therefore, reconciling high black hole masses with close orbital separations is a major challenge for binary evolution models.

In the standard picture, such systems involve a common-envelope phase, which would naturally lead to a merger (Podsiadlowski, Rappaport & Han 2003). Alternatively, de Mink et al. (2009) propose that the short orbital period results in tidal-locking of the stellar rotation, causing a chemically homogeneous evolution through rotational mixing (Maeder 1987). In this scenario, binary components would remain compact and so circumvent the high mass transfer rates of Roche-lobe overflow systems.

If NGC 300 X-1 and IC 10 X-1 were to survive their second supernova explosion, they would form binary black hole systems, merging on a time-scale of a few Gyr. Binary black hole mergers have been considered by Sadowski et al. (2008), who argued that their detection rate may be much higher than double neutron star systems for current gravitational wave experiments.

In conclusion, new VLT/FORS2 time-series spectroscopy of the WN star #41 in NGC 300 is presented, which confirm that it is physically associated with the NGC 300 X-1 system. We find that NGC 300 X-1 hosts the most massive stellar-mass black hole known, with the exception of the other extragalactic WR/black hole system IC 10 X-1.

ACKNOWLEDGMENTS

We wish to thank John Hillier for maintaining CMFGEN and the referee for suggesting improvements to the original manuscript.

REFERENCES

Barnard R., Clark J. S., Kolb U. C., 2008, A&A, 488, 697
Belczynski K., Bulik T., Fryer C. L., Ruiter A., Vink J. S., Hurley J. R., 2009, ApJ, submitted (arXiv:0904.2784)
Bresolin F., Gieren W., Kudritzki R.-P., Pietrzynski G., Urbaneja M. A., Carraro G., 2009, ApJ, 700, 309
Carpano S., 2006, PhD thesis, Universität Tübingen
Carpano S., Pollock A. M. T., Wilms J., Ehle M., Schirmer M., 2007a, A&A, 461, L9
Carpano S., Pollock A. M. T., Prestwich A., Crowther P., Wilms J., Yungelson L., Ehle M., 2007b, A&A, 466, L17
Clark J. S., Crowther P. A., 2004, A&A, 414, L45
Crowther P. A., Drissen L., Abbott J. B., Royer P., Smartt S. J., 2003, A&A, 404, 483
Crowther P. A., Carpano S., Hadfield L. J., Pollock A. M. T., 2007, A&A, 469, L31
de Mink S. E., Cantiello M., Langer N., Pols O. R., Brott I., Yoon S.-Ch., 2009, A&A, 497, 243
Dworetsky M. M., 1983, MNRAS 203, 917
Eggleton P. P., 1983, ApJ 268, 368
Ergma E., Yungelson L. R., 1998, A&A, 33, 151
Fisher R. A., 1935, The Design of Experiments. Hafner, New York
Garnett D., 1990, ApJ, 363, 142
Gieren W., Pietrzynski G., Soszynski I., Bresolin F., Kudritzki R.-P., Minniti D., Storm J., 2005, ApJ, 628, 695
Gies D. R. et al., 2003, ApJ, 583, 424
Hamann W.-R., Koesterke L., Wessolowski U., 1995, A&AS, 113, 459
Hamann W.-R., Gräfener G., Liermann A., 2006, A&A, 457, 1015
Hillier D. J., Miller D. L., 1998, ApJ, 496, 407
Maeder A., 1987, A&A, 178, 159
Magrini L., Vilchez J. M., Mampaso A., Corradi R. L. M., Leisy P., 2007, A&A, 470, 865
Mokiem M. R. et al., 2007, A&A, 473, 603
Orosz J. A. et al., 2001, ApJ, 555, 489
Orosz J. A. et al., 2007, Nat, 449, 872
Orosz J. A., Steeghs D., McClintock J. E., 2009, ApJ, 697, 573
Podsiadlowski P., Rappaport S., Han Z., 2003, MNRAS, 341, 385
Press W. H., Rybicki G. B., 1989, ApJ, 338, 277
Prestwich A. H. et al., 2007, ApJ, 669, L21
Remillard R. A., McClintock J. E., 2006, ARA&A, 44, 49
Russell S. C., Dopita M. A., 1990, ApJS, 74, 93
Sadowski A., Belcyznski K., Bulik T., Ivanova N., Rasio F. R., O'Shaughnessy R., 2008, ApJ, 676, 1162
Schaerer D., Maeder A., 1992, A&A, 263, 129
Schild H., Crowther P. A., Abbott J. B., Schmutz W., 2003, A&A, 397, 859
Shakura N. I., Sunyaev R. A., 1973, A&A, 24, 337
Silverman J. M., Filippenko A. V., 2008, ApJ, 678, L17
Tutukov A., Yungelson L., 1973, Nauchnye Informatsii, 27, 70
Urbaneja M. A. et al., 2005, ApJ, 622, 862
Val-Baker A. K. F., Norton A. J., Negueruela I., 2007, in Di Salvo T., Israel G. L., Piersanti L., Tornambe A., eds, AIP Conf. Ser. Vol. 924, The Multicolored Landscape of Compact Objects and their Explosive Origins. Springer, Heidelberg, p. 530
van den Heuvel E. P. J., de Loore C., 1973, A&A, 25, 387
van Kerkwijk M. H. et al., 1992, Nat, 355, 703
Walborn N. R., Drissen L., Parker J. W., Saha A., MacKenty J. W., White R. L., 1999, AJ, 118, 1684

This paper has been typeset from a TEX/LATEX file prepared by the author.